ELSEVIER

Materials Science and Engineering A 408 (2005) 26–32

MATERIALS SCIENCE & ENGINEERING A

www.elsevier.com/locate/msea

On the relative fraction of ε martensite in γ-Fe–Mn alloys

J. Martínez [a], S.M. Cotes [a,*], A.F. Cabrera [a], J. Desimoni [a], A. Fernández Guillermet [b]

[a] *Departamento de Física, Facultad de Ciencias Exactas, Universidad Nacional de La Plata and Instituto de Física La Plata, CONICET, C.C. 67, 1900 La Plata, Argentina*

[b] *Centro Atómico Bariloche and Instituto Balseiro, and CONICET, Avda. E. Bustillo 9500, 8400 S.C. de Bariloche, Argentina*

Received in revised form 3 June 2005; accepted 17 June 2005

Abstract

Fe–Mn quenched alloys with Mn content between 13 and 27 wt% have been studied using X-ray diffraction, Mössbauer spectroscopy, differential scanning calorimetry and dilatometry. The samples have been structurally characterized using X-ray diffraction and Mössbauer spectroscopy. The composition dependence of the relative fraction of ε phase was determined by dilatometry and Mössbauer spectroscopy. Using a differential scanning calorimeter, measurements of the absorbed heat accompanying the $\varepsilon \rightarrow \gamma$ martensitic transformation were also performed. The relative fractions of ε phase determined by dilatometry agree well with those reported in Schumann's classical work [H. Schumann, Arch. Eisenchüttenw. 38 (8) (1967) 647–656] for Mn contents up to about 22 wt% Mn, but for higher concentrations, a larger fraction was found. The discrepancy was explained in terms of the differences between the present heat treatments and those applied by Schumann. However, relative fractions of ε phase determined by Mössbauer spectroscopy resulted systematically larger than those obtained from dilatometry. On the other hand, independent calculations of the transformation heat were performed for the different compositions. They resulted from multiplying the ε fraction by the calculated $\varepsilon \rightarrow \gamma$ enthalpy change obtained from a recent assessment of the Gibbs functions of the ε and γ phases from literature. Absorbed heat values calculated using the Mössbauer ε fractions, reproduced well the experimental differential scanning calorimetry data, except when a high density of stacking faults are expected in the sample.

Keywords: Phase fractions; Fe–Mn alloys; Martensitic phase transformation; Mössbauer effect; Differential scanning calorimetry

1. Introduction

Stimulated by the possibility of interesting applications of the shape–memory effect, extensive basic and applied research have been performed over the years in the Fe–Mn system [1–5]. In this system, the shape–memory effect is governed by a martensitic transformation between the γ (FCC or "austenite") and the ε (HCP or "martensite") phases. Thus, the design of improved shape–memory alloys depends crucially upon a detailed understanding of the γ/ε transformation.

In the Fe–Mn system, γ is a stable high temperature phase while the ε phase is metastable at all temperatures. In alloys with relatively low Mn content, the $\gamma \rightarrow \varepsilon$ martensitic transformation can be induced by quenching from high temperature [6]. The martensite so obtained is called "thermal" in opposition to that formed by application of stresses [7].

Most of the previously reported experimental studies have been devoted to the determination of the starting temperatures of the direct martensic transformation on cooling (i.e., $\gamma \rightarrow \varepsilon$), and the reverse transformation on heating (i.e., $\varepsilon \rightarrow \gamma$), M_S and A_S, respectively [6,8]. Both M_S and A_S decrease smoothly with increasing Mn content up to a concentration at which these temperatures approach the critical temperature for antiferromagnetic ordering, i.e., the Nèel temperature, T_N^{γ} [6,9]. There, the onset of antiferromagnetic ordering stabilizes the γ phase relatively to ε, and a drastic decrease of M_S and A_S with increasing Mn content is observed.

From a thermodynamic viewpoint, the interesting quantity is the molar Gibbs energy difference between ε and γ phases, $\Delta G_m^{\gamma/\varepsilon} = G_m^{\gamma} - G_m^{\varepsilon}$, which represents the thermodynamic

* Corresponding author. Tel.: +54 221 4246062; fax: +54 221 4252006.
E-mail address: cotes@fisica.unlp.edu.ar (S.M. Cotes).

0921-5093/$ – see front matter © 2005 Published by Elsevier B.V.
doi:10.1016/j.msea.2005.06.019

driving force for the martensitic transformation [10–12]. Since $\Delta G_m^{\gamma/\varepsilon}$ has to be referred to the amount of ε phase actually formed, the martensite relative fraction in quenched alloys is a key quantity in connecting the thermodynamic and structural accounts of the martensitic transformation in this system.

In a classical study based on X-ray diffraction (XRD), dilatometry (D) and metallography techniques, Schumann determined the room temperature (RT) constitution of quenched Fe–Mn alloys as a function of composition [13]. His results might be summarized as follows:

(a) In alloys with Mn contents lower than 10 wt%, only the martensitically formed α' phase (BCC) is obtained at RT. The $\gamma \rightarrow \alpha'$ martensitic transformation produced on cooling from 1273 K inhibits the formation of the ε phase. In this composition range, the M_S temperature of the $\gamma \rightarrow \alpha'$ transformation is higher than that of the $\gamma \rightarrow \varepsilon$ martensitic transformation.
(b) In alloys with Mn content between 10 and 15 wt%, most of the material in the quenched samples presents the α' structure, but the ε phase also occurs at RT. In this case, the M_S temperatures of both the $\gamma \rightarrow \alpha'$ and the $\gamma \rightarrow \varepsilon$ transformations are very close [6].
(c) In alloys with Mn content between 15 and 23 wt%, the amount of ε phase present in the quenched samples varies from 40 to 50%. The rest of the material is untransformed γ phase.
(d) In alloys with Mn contents larger than 23 wt%; the amount of ε phase decreases with increasing Mn concentration. In alloys with more than 27 wt% Mn the ε phase is not detected [13]. However, it should be mentioned that small amounts of ε phase in alloys with more than 27 wt% Mn have been reported [12,14]. The discrepancy has been discussed in terms of the differences in the thermomechanical treatment applied or the detection methods adopted [6].

The present study focuses on the determination of the relative fraction of ε martensite in quenched Fe–Mn alloys, as a function of the Mn content, in the composition range between 13 and 27 wt% of Mn. The relative fractions are obtained by using two complementary techniques, viz., dilatometry and Mössbauer spectroscopy (MS). The relative fraction values, f_D^{ε} and f_M^{ε}, from D and MS experiments, respectively, are then combined with the calculated enthalpy change, $\Delta H^{\gamma/\varepsilon} = H^{\gamma} - H^{\varepsilon}$, extracted from the assessment developed in Ref. [10]. In this way, independent predictions of the absorbed heat (Q) during the $\varepsilon \rightarrow \gamma$ transformation are obtained, which can be straightforward compared with experimental Q data. Additionally, an experimental database is developed based in differential scanning calorimetry (DSC) measurements of the $\varepsilon \rightarrow \gamma$ transformation heat. A comparison between the predicted and experimental data on Q is performed. Finally, with these various pieces of information, a discussion is done on the ε fractions versus composition relation for quenched Fe–Mn alloys.

2. Experimental

2.1. Alloys, samples and heat treatments

Fe and Mn, both of 99.98% purity, were used to prepare the alloys in an arc furnace under Ar atmosphere. The melting procedure has been described in detail elsewhere [15,16]. The resulting alloys weighed about 20 g each. These alloys were encapsulated in a quartz tube with an Ar atmosphere, kept 48 h at 1273 K, and then water-quenched breaking the tube. The chemical composition of the alloys was determined using wavelength dispersion spectrometry with a CAMECA microprobe. The samples were obtained by cutting pieces with a diamond blade-sawing machine. After polishing and clearing the surface of the pieces, an annealing at 950 °C during one hour in a quartz tube filled with Ar was performed, with a subsequent water-quenching without breaking the tube to avoid oxidation. The samples whose M_F temperatures (i.e., the lowest temperature at which the transformation is detected on cooling) fall at or below RT [6] were cooled down to 77 K before performing the experiments.

2.2. Experimental techniques

The XRD measurements were performed in a Philips PW1710 diffractometer using the monochromatic Cu Kα radiation, in Bragg–Brentano's geometry, with a step mode collection of 0.02°, 1s by step, with 2θ ranging from 10° to 100°.

The Mössbauer spectra were taken using a 5 mCi ^{57}Co*Rh* source and recorded in a standard 512 channels constant acceleration spectrometer. The samples were analyzed using conversion electron Mössbauer spectroscopy (CEMS) with a constant flux helium–methane detector. Transmission geometry was also used to study some of the samples. Velocity calibration was performed against a 12-μm thick α-Fe foil. All isomer shifts are referred to this standard at 298 K.

The dilatometric measurements were performed in a homemade dilatometer with a temperature range from 100 to 620 K. In this equipment, a linear variable differential transformer type Hottinger W1E monitors the length of the sample. The resolution used was 10^{-4} mm. Experiments were performed at heating and cooling rates of about 3 K/min. A thermocouple was welded on the surface of the sample.

The calorimetric measurements were performed using a Shimadzu-50 DSC calorimeter. Measurements were performed on heating at a constant rate of 10 K/min in N_2 atmosphere. The maximum temperature reached on heating was 600 K and the minimum temperature of the cooling step was 300 K. Al_2O_3 powder was used as a reference in these measurements.

3. Data processing methods

3.1. Transformation temperatures

In order to determine the A_S and A_F (i.e., the highest temperatures at which the transformation is detected on heating) temperatures, the variations in the slope of the ratio $\Delta L/L_0$, between the variation (ΔL) of the sample length and the initial length (L_0) at RT, were analyzed as a function of temperature. In addition, the A_S and A_F temperatures were obtained from DSC measurements.

3.2. Relative fractions

The relative fractions of the ε phase, f_D^ε and f_M^ε, were determined from $\Delta L/L_0$ versus T curves using the following relation [17]:

$$f_D^\varepsilon = 3\frac{\Delta L^*}{L_S}\frac{V_m^\varepsilon}{V_m^\gamma - V_m^\varepsilon} \quad (1)$$

Here $\Delta L^* = L_F - L_S$, and L_F and L_S are the sample length after (F) and before (S) the transformation, respectively, and were determined from the heating and cooling curves at an intermediate temperature, $T_m = (A_S + A_F)/2$. V_m^γ and V_m^ε are the molar volumes of γ and ε phases, respectively, directly evaluated from available lattice parameter versus composition data for the Fe–Mn γ and ε phases [11,12].

The relative phase fractions were also determined from Mössbauer data. The spectra were fitted using Lorentzian line shapes using a non-linear least-squares program with constraints. The same Mössbauer–Lamb factor was assumed for the various phases. As a result of the fitting procedure, the sub-spectra corresponding to each phase present in the sample are obtained. Phase fraction of each phase is directly the relative area of the corresponding sub-spectra.

3.3. Transformation heat

The measured absorbed heat (Q) associated with the $\varepsilon \rightarrow \gamma$ transformation was evaluated from experimental DSC curves (dQ/dt versus t; t: time) once the base line of the apparatus was subtracted. For alloys whose Néel temperature is close to A_S, after the first heating from RT, the sample was cooled down to a temperature greater than M_S, and then a second measurement was performed on heating. In this second heating step, only the γ phase is present in the sample. Consequently, only the magnetic heat flux due to the antiferromagnetic-to-paramagnetic transformation of γ is detected. Afterwards, the second heating curve multiplied by the relative fraction of the γ phase obtained either by D or MS, was subtracted from the first one. This procedure allows eliminating the magnetic contribution to the signal, as well as the base line of the apparatus. Finally, the absorbed heat associated with the structural transformation was obtained by integrating the area under the curve between $t(A_S)$ and $t(A_F)$. However, these Q values depend on the original ε phase fraction in each sample.

A prediction of the theoretical (th) value for the transformation heat was derived from the assessed enthalpy change, $\Delta H^{\gamma/\varepsilon}$ [10,16], using the following expression:

$$Q_i^{th} = f_i^\varepsilon \Delta H^{\gamma/\varepsilon} \quad (2)$$

where the sub-index i (= D, M) refers to the dilatometric or the Mössbauer measurements, respectively.

4. Results

The XRD patterns obtained for the various samples are presented in Fig. 1. In the diffractogram corresponding to the alloy with 13.7 wt% Mn, diffraction peaks for the ε and α' phases [11] were observed, but only the reflections for the ε and γ phases were detected in alloys with higher Mn contents.

Fig. 2 presents the Mössbauer spectra recorded for the various Mn concentrations. In agreement with the XRD results (Fig. 1), the spectrum of the alloy with 13.7 wt% Mn was analyzed by taking into account the contribution of the ferromagnetic α' phase as well as the ε one. Only the two central lines of the α' sextets at ± 3 mm/s are observed in the low velocity range spectrum. The α' contribution was reproduced with three magnetic interactions, each one associated with a different configuration around the Fe-atom [18]. The resulting α' hyperfine parameters (B_i and δ_i, hyperfine field and isomer shift, respectively) and the relative fractions (f_0, f_1 and f_{2+}) obtained from the high velocity spectrum were: $B_0 = 32.9_1$ T, $\delta_0 = 0.01_1$ mm/s, $f_0 = 0.36_4$; $B_1 = 30.7_1$ T, $\delta_1 = -0.02_4$ mm/s, $f_1 = 0.34_5$; $B_{2+} = 28.1_1$ T,

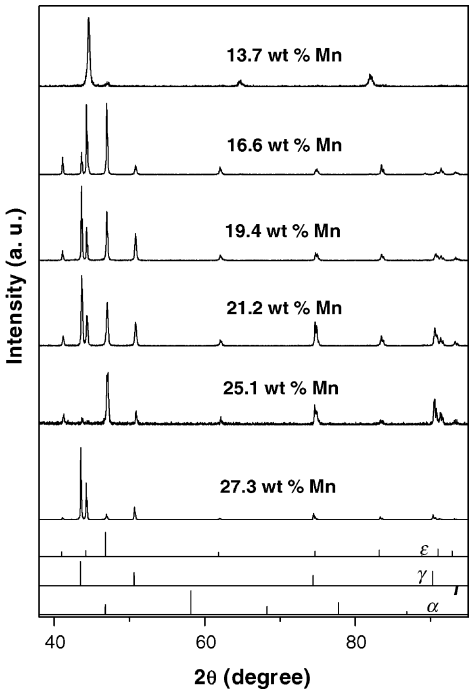

Fig. 1. X-ray diffraction patterns labeled with the Mn contents. The reflections belonging to ε, γ and α' phases, respectively, are indicated at the bottom.

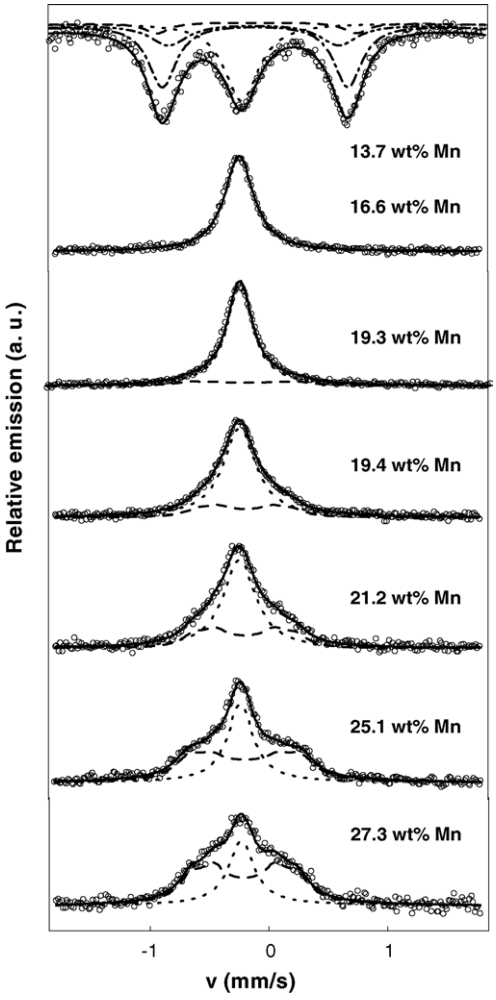

Fig. 2. Mössbauer spectra recorded on samples with different Mn content.

$\delta_{2+} = -0.01_1$ mm/s, $f_{2+} = 0.23_4$, which were associated to Fe probes with 0, 1 and 2 or more near neighbor Mn atoms, respectively. Only the single line of isomer shift δ_ε associated to the paramagnetic ε phase was used to analyze the 16.6 wt% of Mn alloy spectrum. It should be emphasized, however, that the possible existence of a small amount of γ phase in the paramagnetic state also contributing to the spectrum cannot be ruled out. The spectra recorded from higher Mn concentrations alloys (>17 wt%) were satisfactorily described with the hyperfine interactions of γ and ε phases. Since T_N^γ of the present alloys is higher than RT [9], a non-resolved sextet of magnetic hyperfine field B_γ and isomer shift δ_γ was used to describe this antiferromagnetic phase [7]. Table 1 reports the hyperfine parameters and the relative fractions extracted from the analysis of the spectra.

In Fig. 3 some typical $\Delta L/L_0$ versus T curves are presented. The f_D^ε relative fractions, as well as the A_S and A_F temperatures extracted from these experiments are listed in Table 2.

Fig. 4 shows DSC curves taken on heating. The curves corresponding to 13.7, 16.6, 19.3, 19.4 and 21.2 wt% Mn showed only the structural signal, but at higher Mn content alloys a contribution due to the magnetic transition of γ phase at temperatures close to A_S is also observed in the curves. In Table 3 the experimental Q values are reported.

Table 1
Relative fractions (f_M^γ and f_M^ε), hyperfine magnetic field (B^γ) and isomer shift (δ^γ and δ^ε) obtained by analyzing the Mössbauer spectra

Mn (wt%)	δ^ε (mm/s)	f_M^ε	B^γ (T)	δ^γ (mm/s)	f_M^γ
13.7_2	-0.12_1	0.07_1	–	–	–
16.6_5	-0.14_1	1.00_2	–	–	–
19.3_5	-0.13_1	0.88_1	2.8_1	0.09_1	0.11_1
19.4_5	-0.14_1	0.78_3	2.4_1	0.09_1	0.22_2
21.2_4	-0.13_1	0.66_4	2.7_1	0.09_1	0.34_2
25.1_6	-0.13_1	0.44_2	2.9_1	0.09_1	0.56_6
27.3_3	-0.13_1	0.35_3	2.8_1	0.10_1	0.65_7

The errors are quoted as sub-index.

Table 2
Relative fraction of ε phase and A_S and A_F temperatures extracted from the present dilatometric curves

Mn (wt%)	A_S (K)	A_F (K)	f_D^ε
13.7_2	481_9	606_3	0.28_2
16.6_5	488_5	550_6	0.60_1
19.3_5	464_4	495_2	0.52_1
19.4_5	472_3	524_2	0.69_1
21.2_4	462_4	506_4	0.56_1
24.7_8	433_5	467_3	0.50_2
25.1_6	404_5	455_3	0.12_1
26.5_1	403_7	447_3	0.30_1
27.3_3	417_2	450_2	0.17_1

The errors are quoted as sub-index.

Table 3
The absorbed transformation heat, Q, obtained from DSC measurements compared with the Q_i^{th} values with i (= D, M) calculated by inserting in Eq. (2) the ε relative fractions obtained from either, dilatometry and the Mössbauer measurements

Mn (wt%)	Q (J/g)	Q_M^{th} (J/g)	Q_D^{th} (J/g)
16.6_5	16.6_1	25.0_6	15.0_4
19.3_5	17.9_4	20.0_4	12.0_3
19.4_5	17.3_3	18.0_3	16.0_3
21.2_4	14.3_1	14.0_3	12.0_2
25.1_6	7.3_1	7.0_1	2.0_1
27.3_3	3.7_1	5.0_1	2.0_1

The errors are quoted as sub-index.

5. Discussion

The A_S temperatures determined by D and by DSC measurements (filled symbols) are compared in Fig. 5 with previously reported data (open symbols) [17] and with values calculated using the model developed in Ref. [16]. A reasonably good agreement is observed between the present and the previously reported D values. The A_S temperatures from DSC follow the general trend but they are systematically lower, probably due to the higher sensitivity of the DSC technique to detect the start of the transformation compared with D.

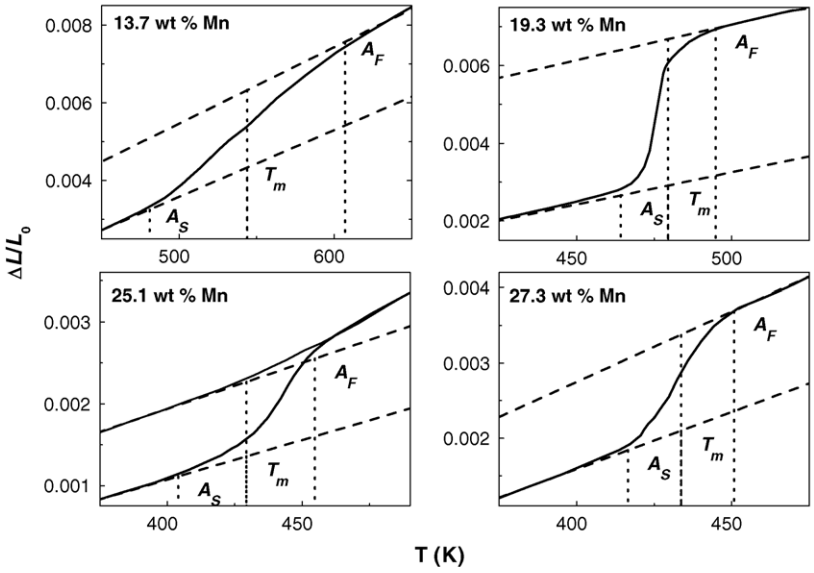

Fig. 3. Dilatometric curves labeled with the Mn content. A_S, A_F and T_m temperatures are also indicated.

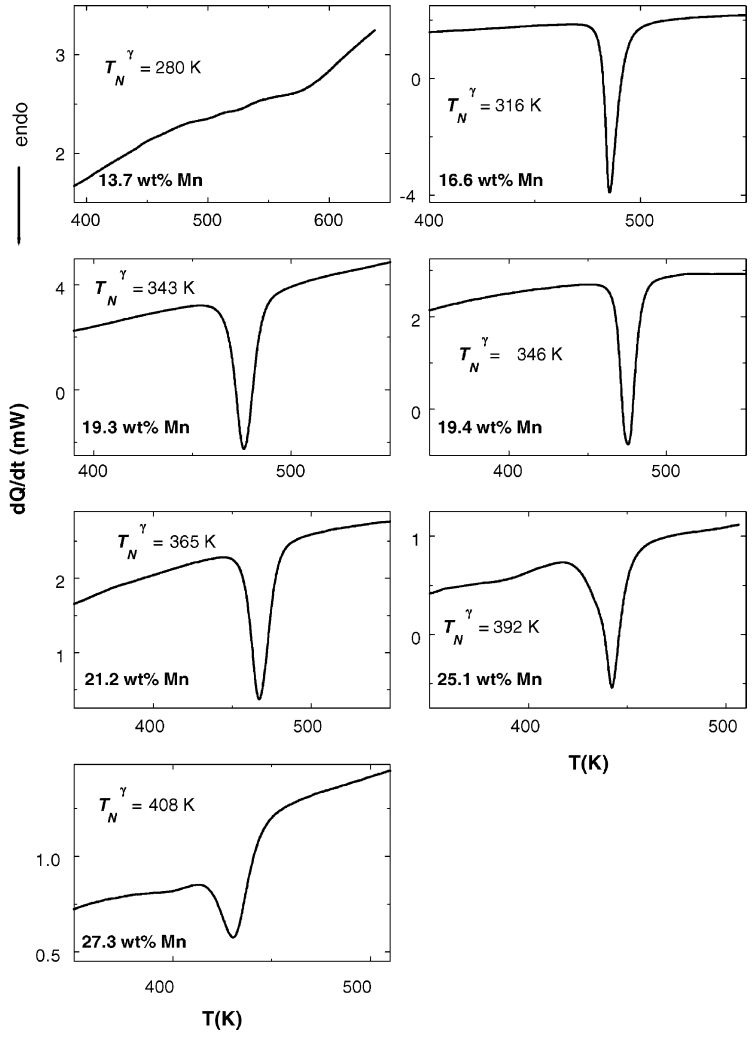

Fig. 4. Calorimetric DSC curves recorded on samples with different Mn content. The Nèel temperature T_N^γ of the corresponding alloy is indicated.

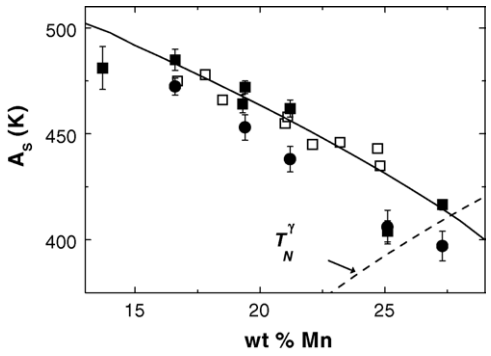

Fig. 5. Composition dependence of the A_S temperature obtained from: (a) filled circle: the present calorimetric measurement, (b) filled square: the present dilatometric measurements and (c) open square: data taken from Ref. [17]. The solid line corresponds to the calculated A_S vs. composition line [16] and the dashed line represents the composition dependence of Nèel temperature T_N^γ [9].

The relative fractions of the ε phase obtained from D measurements (filled symbols) are compared in Fig. 6 with those obtained by Schumann [13] (solid lines) and Marinelli et al. [17] (open symbols). In general, our results indicate a larger fraction of ε phase than the previously reported ones [13,17], which will be discussed in the following. The difference between the present results and those in Ref. [17] might be attributed to the different method of evaluating phase fraction of ε phase from the dilatometric curves. The differences between our results and those in Ref. [13], in particular for those alloys in the region with more than 22 wt% Mn, might be ascribed to differences in the adopted heat treatments applied to the samples. In the present work, the alloys with M_F temperatures lower than RT [6,15] were cooled down to 77 K in order to obtain the maximum possible amount of ε phase. This procedure was not followed in Ref. [13].

The relative fractions of ε phase obtained from D measurements and from MS are compared in Fig. 7. The f_M^ε are systematically and significantly larger than f_D^ε, and the difference between them decreases with increasing Mn content. We shall now argue that this discrepancy might be associated with the different characteristic scales probed by these techniques,

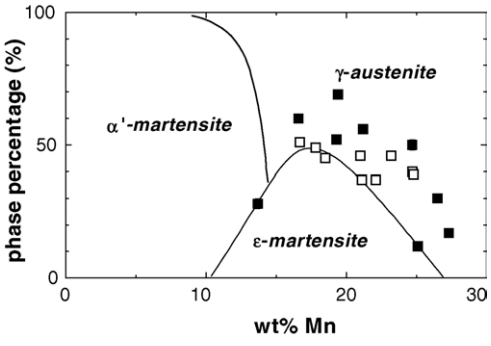

Fig. 6. Relative fractions determined by dilatometry on samples quenched from 1273 K. (a) Filled square: present work and (b) open square: Ref. [17]. The solid lines describe the fractions of the various phases according to Ref. [13].

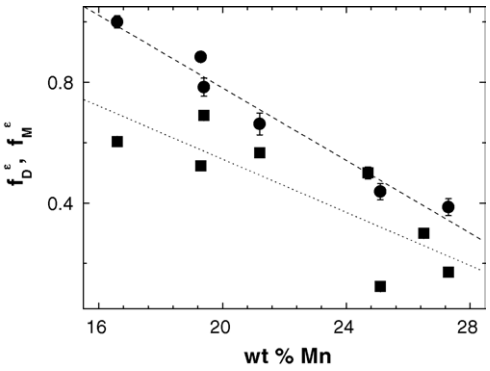

Fig. 7. Relative fractions of the ε phase determined in the present work from: (a) dilatometric measurements (filled square) and (b) Mössbauer spectroscopy (filled circle).

as well as to the rather general features of the γ/ε martensitic transformation in the Fe–Mn system. MS is a nanoscopic technique that investigates a few atomic distances around ^{57}Fe probes. Then, the stacking-faults, which are expected to be present in the γ phase, might be counted by the Mössbauer technique as ε regions leading to an overestimation of the relative fractions of ε martensite. In this view, the effect would be more important for Mn concentrations where the stacking-fault energy is relatively low, i.e., for alloys containing about 15 wt% Mn [8]. On the other hand, in order to account quantitatively for the difference between the dashed and dotted lines in Fig. 7, this mechanism would require a non-plausible large amount of faulted material. Contrasting with this, the D technique detects macroscopic changes, caused by the $\varepsilon \rightarrow \gamma$ transformation, involving a considerable expansion of the interatomic distances, especially in the "c" axis direction of ε structure [8]. In a thermally induced martensitic transformation, various crystallographically equivalent variants of martensite are formed inside each grain [19]. In the reverse transformation, these domains of ε martensite must transform inside the austenite matrix. Then, due to differences in the elastic constants of both phases, the volume change due to the retransformation could probably be affected. Consequently, the macroscopic volume change could result lower

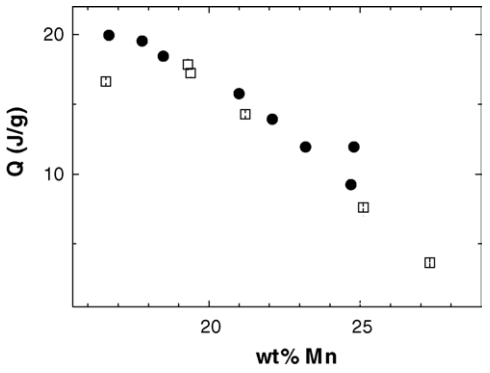

Fig. 8. Absorbed heat (Q) associated with the $\varepsilon \rightarrow \gamma$ transformation vs. Mn (wt%) obtained from DSC measurements. (a) Filled circle: present work and (b) open square: Ref. [17].

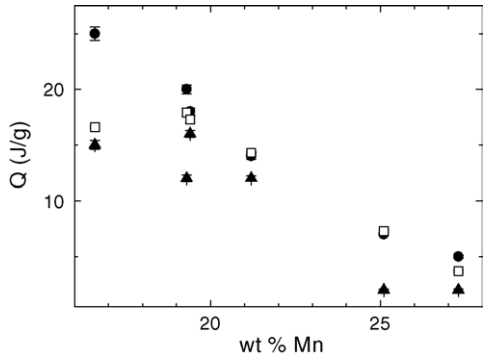

Fig. 9. Absorbed heat associated with the $\varepsilon \rightarrow \gamma$ transformation vs. Mn (wt%). The experimental value (Q) is compared with the calculated ones using the enthalpy change [16] and the ε phase fractions obtained either by MS or by D, respectively. (a) Open square: DSC results, (b) filled circle: calculated using $f_{\mathrm{M}}^{\varepsilon}$ and (c) triangle up: calculated using $f_{\mathrm{D}}^{\varepsilon}$.

than the expected, leading to an underestimation of the ε relative fraction.

The composition dependence of the Q values, according to the present measurements (filled symbols) and those reported in Ref. [14], is presented in Fig. 8. The agreement between these two datasets is excellent within experimental error, except for a single measurement corresponding to the lowest Mn concentration.

In order to further test the present ideas, we will consider the information in Table 3, which comes from DSC, D and MS measurements. A graphical comparison, presented in Fig. 9, indicates that the Q^{th} values estimated thermodynamically by applying Eq. (1) reproduce reasonably well the experimental ones only when the $f_{\mathrm{M}}^{\varepsilon}$ Mössbauer relative fractions are inserted in Eq. (1). Indeed, a discrepancy between experiments and calculations is noted for the alloy with 16.6 wt% Mn. Of course, in this particular case the $f_{\mathrm{M}}^{\varepsilon}$ might in fact be enhanced by the presence of a small amount of faulted γ phase.

Additional experimental and theoretical work is necessary to fully understand the striking discrepancy.

6. Summary and conclusions

A systematic study of the relative fraction of the ε martensite phase in quenched Fe–Mn alloys has been performed, using two alternative methods, viz., Mössbauer spectroscopy and the combination of dilatometry and lattice parameter data for the individual phases. A significant composition-dependent discrepancy has been detected. Possible explanations of this effect, which take into account the concentration of stacking-faults in the untransformed γ phase and the transformation of the martensite variants inside the austenite matrix have been considered. An indirect support to the present results was obtained by predicting the absorbed transformation heat. The measured DSC values are reproduced only when the Mössbauer fractions are adopted in the calculation.

Acknowledgements

Ing.C. Ayala and technicians P. Riquelme and T. Carrasco helped us with sample preparation. Research grants from Consejo Nacional de Investigaciones Científicas y Técnicas (CONICET, Argentina), Fundación Rocca and Fundación Antorchas of Argentina are gratefully acknowledged. A.F.G. also acknowledges the support by CONICET, under grant PIP No. 02612.

References

[1] T. Schneider, M. Acet, B. Rellinghaus, E. Wassermann, W. Pepperhoff, Phys. Rev. B 51 (14) (1995) 8917–8921.
[2] A. Baruj, S. Cotes, M. Sade, A. Fernández Guillermet, Z. Metallkd 87 (1996) 765–771.
[3] A. Borgenstam, M. Hillert, J. Phys. IV 7 (1997) C5:23–C5:28.
[4] A. Baruj, A. Fernández Guillermet, M. Sade, Mater. Sci. Eng. A 273–275 (1999) 507–511.
[5] S.M. Cotes, A. Fernández Guillermet, M. Sade, Mater. Sci. Eng. A 273–275 (1999) 503–506.
[6] S. Cotes, M. Sade, A. Fernández Guillermet, Metall. Mater. Trans. A 26A (1995) 1957–1969.
[7] F. Gauzzi, B. Verdini, G. Principi, B. Badan, J. Mater. Sci 18 (1983) 3661–3670.
[8] S.M. Cotes, M. Sade, A. Fernández Guillermet, Metall. Mater. Trans. A 35A (2004) 83–91.
[9] W. Huang, CALPHAD 13 (1989) 243–252.
[10] S. Cotes, A. Baruj, M. Sade, A. Fernández Guillermet, J. de Phys. IV 5 (C2) (1995) 83–88.
[11] P. Marinelli, A. Baruj, M. Sade, A. Fernández Guillermet, Z. Metallkd. 91 (11) (2000) 957–962.
[12] P. Marinelli, A. Baruj, M. Sade, A. Fernández Guillermet, Z. Metallkd. 92 (5) (2001) 489–493.
[13] H. Schumann, Arch. Eisenchüttenw. 38 (8) (1967) 647–656.
[14] B. Skrotzki, Ph. D. Thesis, Fortshitt-Berichte VDI 5, 269, Düsseldorf VDI-Verlag, 1992.
[15] S.M. Cotes, A. Fernández Guillermet, M. Sade, J. Alloys Compd. 280 (1998) 168–177.
[16] S.M. Cotes, A. Fernández Guillermet, M. Sade, J. Alloys Compd. 278 (1998) 231–238.
[17] P. Marinelli, A. Baruj, J. Pons, M. Sade, A. Fernández Guillermet, E. Cesari, Mater. Sci. Eng. A 335 (2002) 137–146.
[18] M.A. Dapino, S.M. Cotes, A.F. Cabrera, R. Mercader, J. Desimoni, Hyperfine Interact. 148–149 (2003) 331–336.
[19] S. Kajiwara, Mater. Sci. Eng. A A273–275 (1999) 67–88.